

DNA breathing dynamics: Analytic results for distribution functions of relevant Brownian functionals

Malay Bandyopadhyay¹, Shamik Gupta² and Dvira Segal¹

¹*Chemical Physics Theory Group, University of Toronto,
80, Saint George Street, Ontario M5S 3H6, Canada*

²*Department of Physics of Complex Systems, Weizmann Institute of Science, Rehovot 76100, Israel*
(Dated: February 16, 2022)

We investigate DNA breathing dynamics by suggesting and examining several different Brownian functionals associated with bubble lifetime and reactivity. Bubble dynamics is described as an overdamped random walk in the number of broken base pairs. The walk takes place on the Poland-Scheraga free energy landscape. We suggest several probability distribution functions that characterize the breathing process, and adopt the recently studied backward Fokker-Planck method and the path decomposition method as elegant and flexible tools for deriving these distributions. In particular, for a bubble of an initial size x_0 , we derive analytical expressions for (i) the distribution $P(t_f|x_0)$ of the first-passage time t_f , characterizing the bubble lifetime, (ii) the distribution $P(A|x_0)$ of the area A till the first-passage time, providing information about the effective reactivity of the bubble to processes within the DNA, (iii) the distribution $P(M)$ of the maximum bubble size M attained before the first-passage time, and (iv) the joint probability distribution $P(M, t_m)$ of the maximum bubble size M and the time t_m of its occurrence before the first-passage time. These distributions are analyzed in the limit of small and large bubble sizes. We supplement our analytical predictions with direct numerical simulations of the related Langevin equation, and obtain a very good agreement in the appropriate limits. The nontrivial scaling behavior of the various quantities analyzed here can, in principle, be explored experimentally.

PACS numbers: 87.14.gk, 87.10.Mn, 02.50.-r, 05.40.-a

I. INTRODUCTION

The Watson-Crick double helix structure of DNA derives its stability from the phosphodiester bonds in the single-stranded sugar backbone, and from the hydrogen bonds between complementary base pairs on opposite strands [1, 2]. In practice, access to the inside of the double helix, and therefore, the unzipping of a specific region of base pairs is essential for all physiological processes involving DNA, e.g., for replication, transcription, and protein binding [3].

Several mechanisms, like heating [4], changing the pH of the environment [5], and application of external force [6] can lead to unzipping of the double-stranded DNA. This phenomenon is referred to as DNA denaturation. The process occurs progressively, starting with the double strand separating locally into single strands to form loops, or, “bubbles”. These bubbles fluctuate in size through stepwise zipping and unzipping of the base pairs at the two zipper forks where the bubble connects to the double strand. At low temperatures, bubbles once formed eventually close again in time. With the increase of temperature, however, the bubbles grow in size in time to ultimately coalesce with neighboring bubbles and complete the denaturation process. The melting temperature T_m is defined as that at which half of the DNA molecule is denatured, and has typical values $\sim 70 - 100^\circ\text{C}$ for standard salt solutions [5]. The number of bubbles varies from only a few ones well below T_m up to several hundreds close to T_m .

Breathing dynamics, referring to the dynamics of fluc-

tuating DNA bubbles, has been a topic of intense research for many years [3, 4]. It has recently regained interest with the development of new experimental tools that allow for the direct observation of the dynamics of a single DNA molecule [7, 8]. On the theoretical side, various methods have been used to study different aspects of the breathing process [9, 10], and to investigate the interaction of the DNA with binding proteins: the master equation approach [11, 12], a stochastic Gillespie scheme [13], the Fokker-Planck equation approach based on the Poland-Scheraga free energy function [5, 14–16], and stochastic dynamic simulations based on the Dauxios-Peyrard-Bishop model [17, 18]. Specifically, the thermally-induced denaturation problem has been recently studied by mapping it onto a quantum Coulomb problem [19, 20]. These studies have enhanced our understanding of general aspects of both polymer dynamics as well as specific biochemical processes. For recent advances, see [9].

DNA breathing occurs on a timescale shorter than the equilibration time of the single strands forming the bubbles [8]. Based on this observation, breathing dynamics may be regarded as a random walk in the one-dimensional coordinate x , the number of broken base pairs. Ignoring heterogeneity in the DNA structure, this random walk may be modeled as a noisy overdamped motion at a finite temperature T on the Poland-Scheraga free energy landscape, $\mathcal{F}(x) \sim \gamma x + ck_B T \ln x$ [10, 19]. The parameters $c > 0$ and γ (which can be of either sign) are defined later in the paper. As we show below, this form of the free energy implies a crossover scale x_{ch} . For small bubbles ($x < x_{\text{ch}}$), the random walk takes

place in a potential $\sim \ln x$. In the opposite limit, the potential grows linearly with x , thereby implying a different dynamics. Furthermore, the sign of γ , as given by the system temperature, determines the nature (attractive/repulsive) of the potential. For $\gamma > 0$, which happens at temperatures $T < T_m$, the potential is attractive for all bubble sizes, thereby implying an eventual bubble closure ($x = 0$). On the other hand, above T_m , when $\gamma < 0$, a large bubble ($x > x_{\text{ch}}$) evolves under a repulsive linear potential to grow in size toward full denaturation, while a small bubble ($x < x_{\text{ch}}$) may still shrink in size to closure under the influence of the attractive $\ln x$ potential.

In this work, following the above picture, we complement previous single-bubble studies by suggesting and analyzing new measures for exploring the DNA breathing process. We focus on several first-passage “Brownian” functionals [21] of the fluctuating bubble, which eventually closes again, and derive their probability distribution functions (pdfs). We separately study the small and large bubble limits, which exhibit different behaviors. The functionals of interest characterize the lifetime of the bubble, the time-integrated bubble size till the first-passage time (the bubble “area”), its maximum size before closure, and the characteristic time for attaining the maximum size. These measures are relevant for estimating the effective reactivity of the bubble, e.g., its efficiency for binding processes.

Another objective of this work is to advocate the use of the recently studied backward Fokker-Planck (BFP) method [22] and the path decomposition (PD) method [23], which builds on the Feynman-Kac formalism [24], for exploring DNA bubble dynamics. These techniques have been extremely useful in studying many aspects of classical Brownian motion, as well as for exploring related problems in computer science and astronomy [22, 25, 26]. Here, for the first time, we adopt these elegant methods in the context of DNA breathing dynamics. Using the BFP method, we derive and solve differential equations for the Laplace transforms of various Brownian functionals. This is in contrast to the standard Fokker-Planck treatment, which yields the distribution function to obtain a bubble of a given size at a given time [14–16, 18]. Utilizing the PD approach, we can calculate the distribution functions of interest by splitting a representative path of the dynamics into parts, and then considering the weight of each part separately. This is justified by the Markovian property of the dynamics.

In order to gain a qualitative understanding of the DNA breathing process, we separately consider the cases of small and large bubbles. Our analysis reveals new scaling laws for the pdfs of various Brownian functionals, which are evidently distinct for small and large bubbles. We further compare our analytical predictions with direct numerical simulations of the corresponding Langevin equation and observe a very good agreement in the appropriate limits.

The paper is organized as follows. In Section II, we

recall the random walk model and discuss the distribution functions of interest and their relevance to the DNA dynamics. The BFP and the PD methods are also explained, along with a short description of the numerical technique adopted. In Section III, we study the dynamics of small bubbles, and derive the probability distribution functions of several first-passage Brownian functionals. In Section IV, the dynamics of large bubbles is examined. We draw our conclusions in Section V.

II. MODEL, QUANTITIES OF INTEREST, AND METHODS

A. Model

We follow the Poland-Scheraga approach, and interpret bubbles as occurring due to free-energy changes to the double-helical ground state [5]. Measuring the size of a bubble by the number of broken base pairs, and denoting this number by the continuous variable $x \geq 0$, the Poland-Scheraga free energy is given by [5]

$$\mathcal{F}(x) = \gamma_0 + \gamma x + ck_B T \ln x, \quad (1)$$

where γ_0 is the free energy barrier to form the initial bubble, while the term γx stands for the free energy required in breaking x base pairs. The entropy loss in forming a closed polymer loop is taken into account by the term $ck_B T \ln x$, where k_B is the Boltzmann constant, T is the temperature, while c is a universal constant determined by the loop configurations [27]. In Eq. (1), a cutoff at $x \sim 1$ is implied. The parameter γ is assumed to have the simple form, $\gamma = \gamma_1(T_m - T)/T_m$, where $\gamma_1 = 4k_B T_r$, with $T_r = 310\text{K}$ being the reference temperature.

At finite temperatures, the stochastic dynamics of DNA breathing can be modeled by the overdamped Langevin equation [10, 19],

$$\frac{dx}{d\tau} = -D \frac{d\mathcal{F}}{dx} + \xi(\tau). \quad (2)$$

Here, $\xi(\tau)$ is a Gaussian white noise with $\langle \xi(\tau) \rangle = 0$, and $\langle \xi(\tau) \xi(\tau') \rangle = 2Dk_B T \delta(\tau - \tau')$. The kinetic coefficient D has the dimension of $(k_B T)^{-1} s^{-1}$. Using the free energy (1) in Eq. (2), and redefining the time variable, $t \equiv 2Dk_B T \tau$, results in the equation

$$\frac{dx}{dt} = C_2 - \frac{C_1}{x} + \tilde{\xi}(t), \quad (3)$$

where $C_1 = c/2$, $C_2 = \gamma_1(T - T_m)/(2k_B T T_m)$, and

$$\begin{aligned} \langle \tilde{\xi}(t) \rangle &= 0, \\ \langle \tilde{\xi}(t) \tilde{\xi}(t') \rangle &= \delta(t - t'). \end{aligned} \quad (4)$$

Equation (1) implies a crossover scale,

$$x_{\text{ch}} = \frac{C_1}{|C_2|}, \quad (5)$$

such that for small bubbles, $x < x_{\text{ch}}$, the free energy is dominated by the entropic term $\sim \ln x$. Correspondingly, the Langevin dynamics (3) is essentially governed by the term $-C_1/x$. For large bubbles with $x > x_{\text{ch}}$, the base-pair dissociation term $\sim \gamma x$ dominates the free energy, and correspondingly, it is the C_2 term which dictates the Langevin dynamics. For $T < T_m$, the Langevin dynamics occurs in an attractive potential for all bubble sizes, thereby ensuring eventual bubble closure. Above T_m , large bubbles with $x > x_{\text{ch}}$ grow in size under a repulsive linear potential to ultimately yield full denaturation, while a small bubble with $x < x_{\text{ch}}$ may evolve towards closure under the influence of the attractive $\ln x$ potential. We will utilize below the length scale (5) in distinguishing between small and large bubbles. Note that at precisely the melting temperature T_m , when $C_2 = 0$ and the characteristic bubble size diverges, the Langevin dynamics becomes identical to that for small bubbles at all temperatures $T \neq T_m$.

Figure 1 depicts several characteristic paths evolving under Eq. (3) by adopting different values of the parameter C_2 with a fixed C_1 . If $|C_2| > C_1$ and $C_2 < 0$ (i.e., $T < T_m$), the bubble closes sufficiently fast in comparison to the case $C_2 = 0$ (top panel). In the opposite limit, taking positive values for C_2 , one observes the melting process reflected in the divergence of the first-passage time (bottom panel).

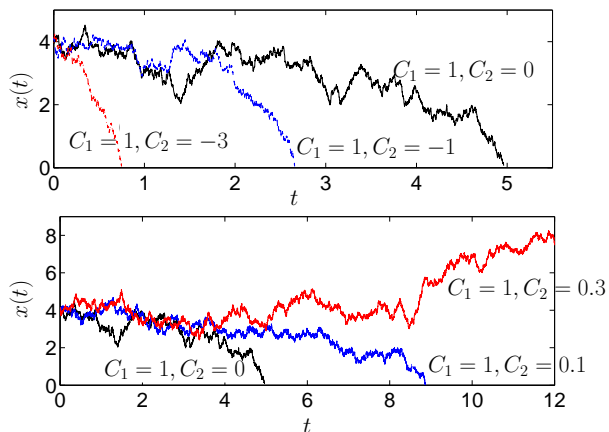


FIG. 1: (Color online) An illustration of several representative paths $x(t)$ following the time evolution of Eq. (3). All the paths begin at $x_0 = 4$. The values of the parameters C_1 and C_2 are marked in the figure. These paths have been generated by using a Brownian simulation (see Section II E).

B. Quantities of interest

Our primary focus is on several first-passage Brownian functionals of experimental relevance. We will consider the following quantities and explore their pdfs for small and large bubbles.

(i) *Bubble lifetime.* The first-passage time pdf $P(t_f|x_0)$

i.e., the pdf of the time of closure for bubbles of initial size x_0 , provides information about bubble lifetime. A related quantity is the survival probability $C(x_0, t) \equiv 1 - \int_0^t P(x_0|t_f) dt_f$ which can be inferred from experiments by measuring fluorescence correlations of a tagged DNA [7, 8].

(ii) *Area under a path.* For the path described by Eq. (3), we define the area under the path before the first-passage time as $A = \int_0^{t_f} x(t') dt'$, see Fig. 2, and calculate its pdf $P(A|x_0)$. This quantity is of interest since it provides a measure for the effectiveness of breathing-assisted processes, i.e., binding of proteins to the reactive sites of the DNA bases. As an example, consider a process that can take place only inside the double helix, on the single-stranded DNA. Let us assume that this process is facilitated with increasing bubble size, and that it requires a sufficiently long bubble lifetime. While the first-passage time distribution provides information about the average bubble lifetime, it does not contain any hint of the average bubble size before closure. Similarly, $P(M)$, the distribution of the maximum bubble opening before closure provides a measure for the bubble size, but it does not inform us about the corresponding timescale. Thus, we propose the pdf $P(A|x_0)$ of the area A covered till the first-passage time as a useful quantity that provides a measure of bubble reactivity by containing information about both size of the bubble and its characteristic lifetime.

(iii) *Maximum bubble size M .* Another proposed measure for quantifying bubble reactivity is the distribution of the maximum bubble size before the first-passage time, $P(M)$. Consider again a binding process taking place only inside the double helix. Assume next that, due to geometrical constraints, the process may materialize only when the bubble is large enough. If the timescale of this process is very short, shorter than the average bubble lifetime, a relevant measure for the bubble reactivity is its maximum opening before closure.

Quantities (i), (ii) and (iii) will be calculated below by following the backward Fokker-Planck method discussed in Section II C.

(iv) *Maximum size M and the corresponding time t_m .* The joint probability distribution function $P(M, t_m)$ will be investigated here by following the PD method, which builds on the Feynman-Kac formalism [22, 23]; see Section II D. Using this pdf, one can further calculate the distribution function $P(t_m)$ of the time at which the bubble attains its maximum size before closure. This latter pdf is of interest since it provides information about the (average) time of occurrence of the biggest bubble before closure. Processes taking place inside the DNA, facilitated by increased bubble size, will most likely occur around that time.

Figure 2 illustrates a typical path following Eq. (3). The path begins at x_0 and ends at the origin (bubble closure), staying positive in between. The various measures suggested above are also indicated in the figure.

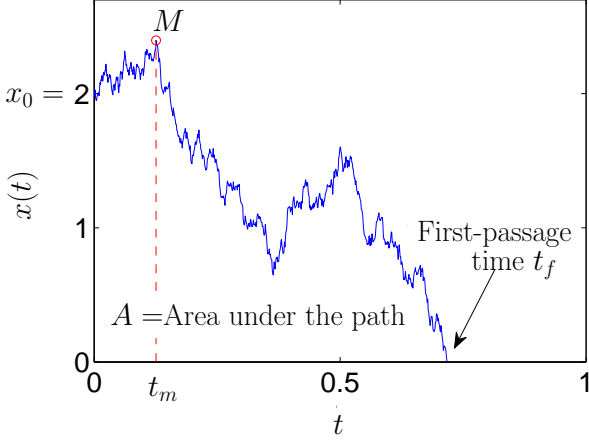


FIG. 2: (Color online) An illustrative path $x(t)$ that begins at x_0 and evolves under Eq. (3). Here, t_f marks the time the path crosses the origin for the first time (corresponding to bubble closure), A is the area enclosed under the path, M and t_m represent respectively the maximum value that the path reaches before the first-passage time, and the corresponding time of occurrence. This path has been generated by using a Brownian simulation (see Section II E) with $C_1 = 1$, $C_2 = -1$, and $x_0 = 2$.

C. The backward Fokker-Planck (BFP) method

Following [22], we recall here how to calculate the statistical properties of a Brownian functional, defined as

$$T = \int_0^{t_f} U(x(\tau)) d\tau. \quad (6)$$

Here, $x(\tau)$ is a path representing the motion (3) which starts at x_0 at time $\tau = 0$ and propagates up to $\tau = t_f$, the first-passage time. In the above equation, $U(x(\tau))$ is a specified function of the path, whose choice depends on the quantity of interest. For example, to compute the distribution of the first-passage time t_f , one chooses $U(x(\tau)) = 1$. For the area distribution till the first-passage time, one should consider $U(x(\tau)) = x$. To find the pdf $P(T|x_0)$, noting that the random variable T can be only positive for these choices of $U(x(\tau))$, one considers its Laplace transform

$$Q(x_0, p) = \int_0^\infty P(T|x_0) e^{-pT} dT = \langle e^{-p \int_0^{t_f} U(x(\tau)) d\tau} \rangle, \quad (7)$$

where the angular brackets denote averaging over all paths starting at x_0 at $\tau = 0$ and ending at the first time they cross the origin. For simplicity of notation, in what follows, we suppress the variable p in the function $Q(x_0, p)$. In order to derive a differential equation for $Q(x_0)$, we follow [22] and split the interval $[0, t_f]$ into two parts. During the first interval $[0, \Delta\tau]$, the path starts from x_0 and propagates up to $x_0 + \Delta x$. In

the second interval $[\Delta\tau, t_f]$, the path starts at $x_0 + \Delta x$ and reaches 0 at t_f . Here, $\Delta\tau$ is a fixed, infinitesimally small time interval. We get, to leading order in $\Delta\tau$, $\int_0^{t_f} U(x(\tau)) d\tau \approx U(x_0) \Delta\tau + \int_{\Delta\tau}^{t_f} U(x) d\tau$, and hence, from Eq. (7),

$$\begin{aligned} Q(x_0) &\approx e^{-pU(x_0)\Delta\tau} \langle Q(x_0 + \Delta x) \rangle_{\Delta x} \\ &\approx (1 - pU(x_0)\Delta\tau) \langle Q(x_0 + \Delta x) \rangle_{\Delta x}. \end{aligned} \quad (8)$$

Now, the average denoted by the angular brackets is performed over all realizations of Δx . The dynamical equation (3) gives $\Delta x = F(x_0)\Delta\tau + \tilde{\xi}(0)\Delta\tau$, with $F(x_0) = C_2 - C_1/x_0$. Substituting for Δx in Eq. (8), expanding $Q(x_0 + \Delta x)$ in powers of $\Delta\tau$, and averaging over the noise by using $\langle \tilde{\xi}(0) \rangle = 0$ and $\langle \tilde{\xi}^2(0) \rangle = 1/\Delta\tau$ for small $\Delta\tau$, one obtains, to lowest order in $\Delta\tau$, the ordinary differential equation,

$$\frac{1}{2} \frac{d^2 Q(x_0)}{dx_0^2} + \left(C_2 - \frac{C_1}{x_0} \right) \frac{dQ(x_0)}{dx_0} - pU(x_0)Q(x_0) = 0. \quad (9)$$

Boundary conditions. The above equation is valid for $x_0 \in [0, \infty]$ with the following boundary conditions: (i) For an infinitesimally small bubble, $x_0 \rightarrow 0$, the first passage time vanishes, $t_f \rightarrow 0$, so that $Q(x_0 = 0) = 1$. (ii) If the bubble is initially large, $x_0 \rightarrow \infty$, the first passage time diverges, hence, $Q(x_0 \rightarrow \infty) = 0$.

We emphasize that the differential equation (9), referred to as the backward Fokker-Planck equation [22], directly provides us with the Laplace-transformed pdfs of various quantities which are determined by the choice of $U(x)$. In contrast, the standard Fokker-Planck method adopted in [14–16, 18] yields the *density* distribution function $P(x, t)$ to obtain a loop of size x at time t . Thus, these two approaches are distinct, providing complementary information.

D. The path decomposition (PD) method

The principle of this technique is simple: Since the motion in Eq. (3) is Markovian, a typical path can be split into, e.g., two parts. Then, the weight of the whole path is the product of the weights of the two split parts [23].

The above idea allows us to calculate the joint probability distribution $P(M, t_m)$ of the maximum bubble size M and the time t_m at which this maximum occurs before closure, given that the initial size of the bubble is fixed at $x_0 \in [0, M]$. By integrating over M , one can further obtain the marginal distribution $P(t_m)$. We compute $P(M, t_m)$ by splitting a typical path into two parts, before and after t_m , with the respective weights W_L and W_R , so that the weight W of the whole path is

$$W = W_L \times W_R. \quad (10)$$

On the left side of t_m , the path propagates from x_0 at $t = 0$ to $M - \epsilon$ at $t = t_m$, without ever attaining the value 0

or M during the interval $[0, t_m]$ [28]. The weight W_L can be determined by using a path integral treatment based on the Feynman-Kac formalism, as we explain below. On the right side of t_m , the path starts from $M - \epsilon$ at $t = t_m$ and ends at the origin at t_f (with $t_f \geq t_m$), without crossing either the level M or the level 0 in between. At the end of the calculation, one needs to take the limit $\epsilon \rightarrow 0$.

The calculation of W_R will be explained in Sections

III D and IV D. We explain here in some detail the calculation of W_L . Since the white noise in Eq. (3) is Gaussian, the probability of a path is given by

$$P[\{x(\tau)\}] \propto \exp \left[-\frac{1}{2} \int_0^t d\tau \left(\frac{dx}{d\tau} + \frac{C_1}{x} - C_2 \right)^2 \right]. \quad (11)$$

The weight W_L is then given as a sum over contributions from all possible paths,

$$\begin{aligned} W_L &\propto \int_{x(0)=x_0}^{x(t_m)=M-\epsilon} \mathcal{D}x(\tau) \exp \left[-\frac{1}{2} \int_0^{t_m} d\tau \left(\frac{dx}{d\tau} + \frac{C_1}{x} - C_2 \right)^2 \right] \prod_{\tau=0}^{t_m} \theta[x(\tau)] \prod_{\tau=0}^{t_m} \theta[M - x(\tau)] \\ &= \left(\frac{x_0}{M - \epsilon} \right)^{C_1} e^{C_2(M - \epsilon - x_0)} \int_{x(0)=x_0}^{x(t_m)=M-\epsilon} \mathcal{D}x(\tau) \exp \left[-\int_0^{t_m} d\tau \left\{ \frac{1}{2} \left(\frac{dx}{d\tau} \right)^2 + \frac{1}{2} \left(\frac{C_1}{x} - C_2 \right)^2 \right\} \right] \prod_{\tau=0}^{t_m} \theta[x(\tau)] \prod_{\tau=0}^{t_m} \theta[M - x(\tau)]. \end{aligned} \quad (12)$$

In the above equations, the terms $\prod_{\tau=0}^{t_m} \theta[x(\tau)]$ and $\prod_{\tau=0}^{t_m} \theta[M - x(\tau)]$ enforce the requirements that the path does not cross either the level 0 or the level M for times between 0 and t_m . Following Feynman-Kac [24], the path integral in Eq. (12) is identified with the propagator $\langle M - \epsilon | e^{-\hat{H}t_m} | x_0 \rangle$, corresponding to the quantum Hamiltonian \hat{H} of a single particle of unit mass,

$$\hat{H} = -\frac{1}{2} \frac{d^2}{dx^2} + V(x), \quad (13)$$

with $\hbar = 1$. The potential energy $V(x)$ is given by

$$V(x) = \begin{cases} \frac{1}{2} \left(\frac{C_1}{x} - C_2 \right)^2 & \text{if } 0 < x < M, \\ \infty & \text{if } x = 0 \text{ or } x = M. \end{cases} \quad (14)$$

Note that the infinite potential energy at $x = 0$ and at $x = M$ enforces the requirement that the path never crosses either the level 0 or the level M . Finally, we get

$$\begin{aligned} W_L &\propto \left(\frac{x_0}{M - \epsilon} \right)^{C_1} e^{C_2(M - \epsilon - x_0)} \langle M - \epsilon | e^{-\hat{H}t_m} | x_0 \rangle \\ &= \left(\frac{x_0}{M - \epsilon} \right)^{C_1} e^{C_2(M - \epsilon - x_0)} \sum_{p=1}^{\infty} e^{-E_p t_m} \psi_p(M - \epsilon) \psi_p(x_0), \end{aligned} \quad (15)$$

where $\psi_p(x)$ and E_p are the eigenfunctions and eigenenergies, respectively, of the Hamiltonian \hat{H} in Eq. (13). As a result of the infinite potential barrier at $x = 0$ and at $x = M$, the eigenfunctions satisfy $\psi_p(x = 0, M) = 0$.

E. Simulations

The statistical properties of Brownian functionals studied here can be numerically obtained by integrating the overdamped Langevin equation (3). Using a second-order stochastic Runge-Kutta algorithm [29], we update the trajectory by following the rule,

$$\begin{aligned} x(\Delta t) &= x_0 + \frac{1}{2} [F(x_0) + F(x_0 + F(x_0)\Delta t + \Gamma_0)] \Delta t \\ &\quad + \Gamma_0, \end{aligned} \quad (16)$$

where $F(x) = C_2 - C_1/x$. Here, Γ_0 is a random number sampled from a Gaussian distribution with zero mean and width given by $\langle \Gamma_0^2 \rangle = \Delta t$. For all simulations presented in this work, we take $\Delta t = 10^{-3}$, unless stated otherwise. We generate a large set of paths, all starting at a particular x_0 and ending close to the origin (within a preassigned numerical tolerance value). Averaging over an ensemble, we generate various pdfs which we compare with our analytical results.

III. SMALL BUBBLE DYNAMICS

We begin our analysis by considering small bubbles, $x < x_{\text{ch}}$, at all temperatures, $T \neq T_m$. The analysis is also valid for bubbles of all sizes at precisely the melting temperature T_m . In these cases, the nonlinear entropic term in the free energy (1) dictates the dynamics, resulting in the Langevin equation,

$$\frac{dx}{dt} = -\frac{C_1}{x} + \tilde{\xi}, \quad (17)$$

where $\langle \tilde{\xi}(t) \rangle = 0$ and $\langle \tilde{\xi}(t)\tilde{\xi}(t') \rangle = \delta(t - t')$. The pdfs $P(t_f|x_0)$ and $P(A|x_0)$ are obtained by the BFP method, where the differential equation that needs to be solved is given by Eq. (9) with $C_2 = 0$,

$$\frac{1}{2} \frac{d^2 Q(x_0)}{dx_0^2} - \frac{C_1}{x_0} \frac{dQ(x_0)}{dx_0} - pU(x_0)Q(x_0) = 0. \quad (18)$$

The boundary conditions are (i) $Q(x_0 \rightarrow \infty) = 0$, and (ii) $Q(x_0 \rightarrow 0) = 1$. We also derive analytical results for $P(M)$ and $P(M, t_m)$, as explained below.

A. First-passage time distribution: $P(t_f|x_0)$

We compute the distribution of t_f , the time at which the bubble closes for the first time, assuming its initial size is fixed at x_0 , by substituting $U(x_0) = 1$ in Eq. (18),

$$\frac{1}{2} \frac{d^2 Q(x_0)}{dx_0^2} - \frac{C_1}{x_0} \frac{dQ(x_0)}{dx_0} - pQ(x_0) = 0. \quad (19)$$

The general solution of Eq. (19) is [30]

$$Q(x_0) = x_0^\alpha \left[AI_\alpha(\sqrt{2px_0}) + BK_\alpha(\sqrt{2px_0}) \right]. \quad (20)$$

Here, $I_\alpha(x)$ and $K_\alpha(x)$ are the modified Bessel functions of the first and second kind, respectively. Also, $\alpha = C_1 + 1/2$, and A and B are arbitrary constants to be determined from the boundary conditions. Since for large x , $I_\alpha(x) \sim e^x/\sqrt{2\pi x}$ and $K_\alpha(x) \sim \sqrt{\pi/2x} e^{-x}$ [31], in order to satisfy the condition $Q(x_0 \rightarrow \infty) = 0$, we must have $A = 0$. To satisfy the condition $Q(x_0 \rightarrow 0) = 1$, we note that as $x \rightarrow 0$, $K_\alpha(x) \approx \Gamma(\alpha)2^{\alpha-1}/x^\alpha$ for $\alpha > 0$ [31], which gives $B = (\sqrt{2p})^{C_1+1/2}/[\Gamma(C_1+1/2)2^{C_1-1/2}]$. Following these considerations, we get the particular solution,

$$Q(x_0) = x_0^{C_1+1/2} \frac{(\sqrt{2p})^{C_1+1/2}}{\Gamma(C_1+1/2)2^{C_1-1/2}} K_{C_1+1/2}(\sqrt{2px_0}). \quad (21)$$

On taking inverse Laplace transform, we get [32]

$$P(t_f|x_0) = \frac{x_0^{2C_1+1}}{\Gamma(C_1+1/2)2^{C_1+1/2}} t_f^{-C_1-3/2} e^{-x_0^2/2t_f}, \quad (22)$$

as obtained earlier in [19, 33].

Next, we compare the analytical prediction (22) with numerical simulations under the *full* bubble potential, including the C_2 contribution, in order to explore the regime of validity of the above result, see the top panel of Fig. 3. The sampled trajectories all begin at $x_0 = 2$. When $x_{\text{ch}} = C_1/|C_2| \gtrsim 10 > x_0$; $C_2 < 0$, we observe a good agreement between numerics and analytical results. For $x_0 \sim x_{\text{ch}}$, deviations occur since then the contribution of C_2 cannot be neglected (inset).

Besides the distribution (22), other related quantities of experimental relevance are the moments, $\langle t_f^k \rangle$, obtained from Eq. (22) as

$$\langle t_f^k \rangle = \frac{x_0^{2k}}{2^k} \frac{\Gamma(C_1 - k + 1/2)}{\Gamma(C_1 + 1/2)} \quad \text{for } k > C_1 + 1/2, \quad (23)$$

while $\langle t_f^k \rangle$ diverges for $k < C_1 + 1/2$. Another important quantity is the persistence, or survival probability of the bubble, defined as

$$C(x_0, t) \equiv 1 - \int_0^t P(t_f|x_0) dt_f, \quad (24)$$

where $\int_0^t P(t_f|x_0) dt_f$ sums up the probabilities of all events where the bubble closes in time t . This quantity can be resolved in experiments by measuring fluorescence correlations of a tagged bubble [7, 8]. On plugging Eq. (22) into Eq. (24), we get

$$C(x_0, t) = 1 - \frac{\Gamma(C_1 + 1/2, x_0^2/2t)}{\Gamma(C_1 + 1/2)}, \quad (25)$$

where $\Gamma(s, x) = \int_x^\infty t^{s-1} \exp(-t) dt$ is the upper incomplete gamma function. This result agrees with that reported in [19]. It is easy to derive the following asymptotic behaviors of $C(x_0, t)$: In the limit $t \rightarrow \infty$, one has [19]

$$C(x_0, t) \approx \frac{(x_0^2)^{C_1+1/2}}{(C_1+1/2)\Gamma(C_1+1/2)} t^{-C_1-1/2}, \quad (26)$$

while, in the limit $t \rightarrow 0$, one has

$$C(x_0, t) \approx 1 - \frac{(x_0^2/2)^{C_1-1/2}}{\Gamma(C_1+1/2)} t^{1/2-C_1} e^{-x_0^2/2t}. \quad (27)$$

B. Distribution of the area till the first-passage time: $P(A|x_0)$

The area $A = \int_0^{t_f} x(t') dt'$ under the random motion (17) can tell us about the readiness of the bubble to react. Here, the motion starts at x_0 and continues in time till the first-passage time. Note that the quantity A is not a geometric area, rather its units are length \times time. To compute the related pdf, we substitute $U(x_0) = x_0$ in Eq. (18),

$$\frac{1}{2} \frac{d^2 Q(x_0)}{dx_0^2} - \frac{C_1}{x_0} \frac{dQ(x_0)}{dx_0} - px_0 Q(x_0) = 0, \quad (28)$$

which has the general solution [34],

$$Q(x_0) = x_0^{C_1+1/2} \left[A_1 J_\nu(iz) + A_2 J_{-\nu}(iz) \right]. \quad (29)$$

Here, $z = (2/3)\sqrt{2p} x_0^{3/2}$, $\nu = (2C_1 + 1)/3$, $J_\nu(x)$ is the Bessel function of the first kind, and A_1 and A_2 are arbitrary constants. Using $J_\nu(x) = i^\nu I_\nu(-ix)$, where $I_\nu(x)$ is the modified Bessel function of the first kind [31], gives

$$Q(x_0) = x_0^{C_1+1/2} \left[B_1 I_\nu(z) + B_2 I_{-\nu}(z) \right], \quad (30)$$

where B_1 and B_2 are arbitrary constants. Since for large x , $I_{\pm\nu}(x) \sim e^x/\sqrt{2\pi x}$ [31], to satisfy the boundary condition $Q(x_0 \rightarrow \infty) = 0$, we must have $B_1 = -B_2$.

To satisfy $Q(x_0 \rightarrow 0) = 1$, we note that as $x_0 \rightarrow 0$, one has $I_\nu(x) \approx (x/2)^\nu / \Gamma(\nu + 1)$ [31], which yields $B_2 = \Gamma(1 - \nu)(\sqrt{2p}/3)^\nu$. We thus get

$$\begin{aligned} Q(x_0) &= \left(\frac{z}{2}\right)^\nu \Gamma(1 - \nu) \left[I_{-\nu}(z) - I_\nu(z) \right] \\ &= \left(\frac{z}{2}\right)^\nu \frac{2}{\Gamma(\nu)} K_\nu(z), \end{aligned} \quad (31)$$

where, in obtaining the last relation, we have used the identities, $K_\nu(x) = (\pi/2)[I_{-\nu}(x) - I_\nu(x)]/\sin(\nu\pi)$ and $\Gamma(\nu)\Gamma(1-\nu) = \pi/\sin(\nu\pi)$ [31]. On taking inverse Laplace transform of (31), we obtain the desired pdf [32],

$$P(A|x_0) = \frac{2^{(2C_1+1)/3} x_0^{2C_1+1} \exp(-2x_0^3/9A)}{3^{(4C_1+2)/3} \Gamma((2C_1+1)/3) A^{(2C_1+4)/3}}. \quad (32)$$

This expression nicely reproduces the numerical results obtained by simulating the Langevin equation (3) under the *full* potential with $x_0 < x_{\text{ch}}$ and $C_2 < 0$, see the middle panel of Fig. 3. The inset demonstrates an expected disagreement for larger bubbles with $x_0 \sim x_{\text{ch}}$.

C. Distribution of the maximum before the first-passage time: $P(M)$

How large can the bubble grow before it closes, assuming an initial opening of x_0 ? This question is of interest in estimating the efficiency of processes that can occur inside big loops only. The relevant measure is provided by $P(M)$, the pdf of the maximum bubble size M before its first closure, given that $x_0 \in [0, M]$. We obtain this pdf by following closely the procedure of [23, 35]. We first define a related function. Let $q(x_0)$ be the probability that the motion described by Eq. (17) exits the interval $[0, M]$ for the first time through the origin. Thus, $q(x_0)$ is the cumulative probability that the maximum before the first-passage time is $\leq M$. It is evident that this function satisfies two boundary conditions: (i) $q(0) = 1$, and (ii) $q(M) = 0$. Denoting by $\phi_{\Delta\tau}(\Delta x)$ the distribution function of a small displacement Δx in time $\Delta\tau \rightarrow 0$, it follows from the Markovian property of the dynamics (17) that

$$q(x_0) = \int q(x_0 + \Delta x) \phi_{\Delta\tau}(\Delta x) d(\Delta x). \quad (33)$$

On Taylor expanding $q(x_0 + \Delta x)$ and averaging over $\Delta x = -(C_1/x_0)\Delta\tau + \tilde{\xi}(0)\Delta\tau$, using $\langle \tilde{\xi}(0) \rangle = 0$, $\langle \tilde{\xi}^2(0) \rangle = 1/\Delta\tau$, we get, to leading order in $\Delta\tau$, the equation $[(1/2)(d^2q(x_0)/dx_0^2) - (C_1/x_0)(dq(x_0)/dx_0)]\Delta\tau = 0$. For arbitrary $\Delta\tau$, we obtain

$$\frac{1}{2} \frac{d^2q(x_0)}{dx_0^2} - \frac{C_1}{x_0} \frac{dq(x_0)}{dx_0} = 0. \quad (34)$$

Solving this equation with the above mentioned boundary conditions, we get

$$q(x_0) = 1 - \left(\frac{x_0}{M}\right)^{2C_1+1}. \quad (35)$$

The pdf of interest is obtained by differentiating $q(x_0)$ with respect to M ,

$$P(M) = \frac{(2C_1+1)x_0^{2C_1+1}}{M^{2C_1+2}}; \quad M \geq x_0. \quad (36)$$

In Fig. 3 (bottom), we compare this result with numerical simulations using the full potential. We observe good agreement for $x_0 < x_{\text{ch}}$; $C_2 < 0$, and an expected disagreement for $x_0 \sim x_{\text{ch}}$ (inset).

D. Joint pdf of the maximum M and the corresponding time t_m before the first-passage time: $P(M, t_m)$

To compute the joint probability distribution of the maximum bubble size M and the time t_m at which the maximum occurs before closure, we adopt the PD method, see Section II D and [23]. We split a path evolving under (17) into two parts, before and after the time t_m , with respective weights W_L and W_R . Due to the Markovian property, the weight W of the whole path is given by the product of the weights for the two split parts, $W = W_L \times W_R$. The weight W_R can be obtained from Eq. (35). Recall that W_R is the weight of a path that starts at $M - \epsilon$ at time $t = t_m$ and exits the interval $[0, M]$ for the first time through the origin. On the other hand, $q(x_0)$ in Eq. (35) is the probability for a path starting at $x_0 \in [0, M]$ to exit the interval for the first time through the origin. We thus deduce that $W_R = q(M - \epsilon)$, or,

$$W_R = 1 - \frac{(M - \epsilon)^{(2C_1+1)}}{M^{2C_1+1}} = \frac{(2C_1+1)\epsilon}{M} + \mathcal{O}(\epsilon^2). \quad (37)$$

The second equality is derived by assuming ϵ to be infinitesimal. The weight W_L is obtained from Eq. (15) by substituting $C_2 = 0$,

$$W_L \propto \left(\frac{x_0}{M - \epsilon}\right)^{C_1} \sum_{p=1}^{\infty} e^{-E_p t_m} \psi_p(M - \epsilon) \psi_p(x_0). \quad (38)$$

Here, ψ_p and E_p are the solutions of the eigenequation,

$$\left[-\frac{1}{2} \frac{d^2}{dx^2} + \frac{C_1^2}{2x^2}\right] \psi = E \psi; \quad 0 < x < M, \quad (39)$$

subject to the condition $\psi(x = 0, M) = 0$. The general solution of this equation is

$$\psi_p(x) = A\sqrt{x}J_\alpha\left(\sqrt{2E_p}x\right) + B\sqrt{x}Y_\alpha\left(\sqrt{2E_p}x\right), \quad (40)$$

where $J_\alpha(x)$ and $Y_\alpha(x)$ are the Bessel functions of order α of the first and second kind, respectively, and $\alpha = \frac{1}{2}\sqrt{1 + 4C_1^2}$ [30]. Note that C_1 is real, thus $\alpha > 0$. Since for $x \rightarrow 0$, $Y_\alpha(x) \approx -(\Gamma(\alpha)/\pi)(2/x)^\alpha$ [31], we demand that $B = 0$ for satisfying $\psi(x = 0) = 0$. The other boundary condition results in the discrete eigenvalues E_p such that $\sqrt{2E_p}M = u_{\alpha p}$, where $u_{\alpha p}$ denotes

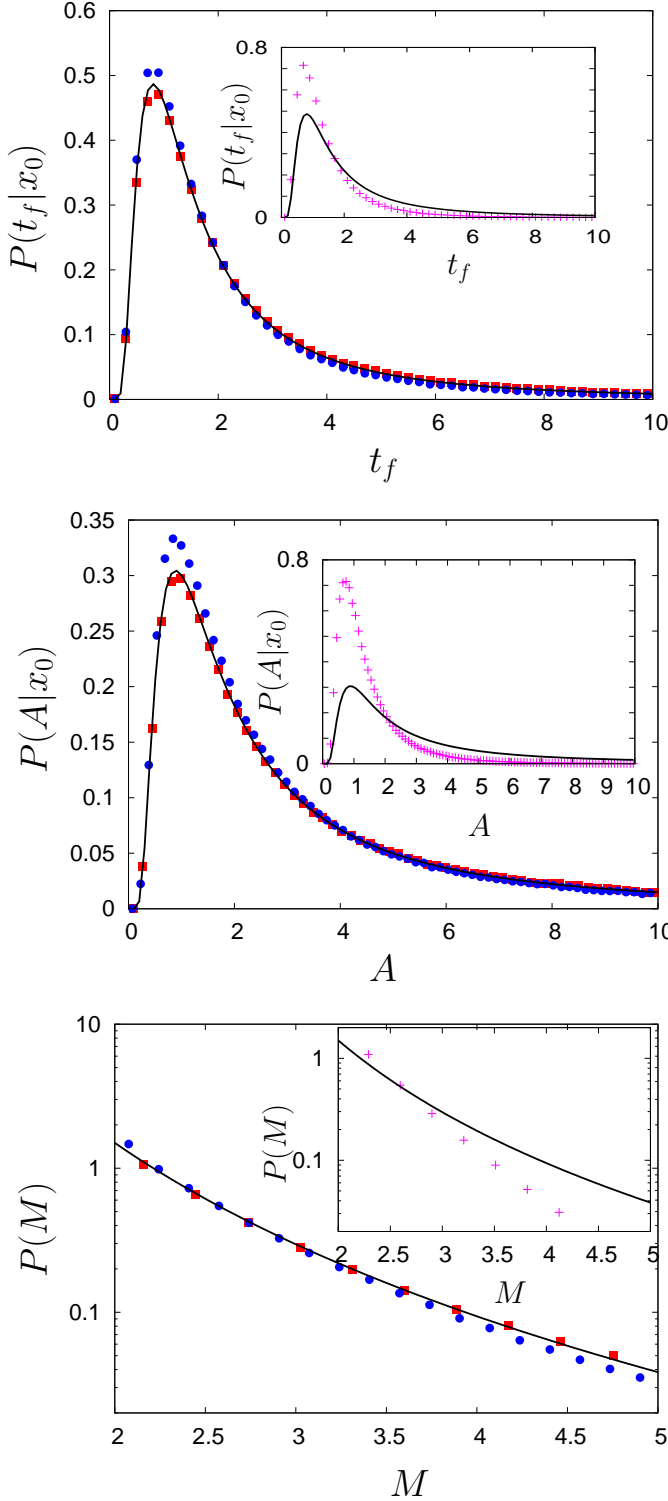


FIG. 3: (Color online) Numerical simulations below the melting temperature, $T < T_m$, for the pdf of the first-passage time (top), the pdf of the area till the first-passage time (center) and the pdf of the maximum size till the first-passage time (bottom). The parameters are $C_1 = 1$ and $C_2 = 0$ (red square), $C_1 = 1$ and $C_2 = -0.1$ (blue dots). The initial bubble size is $x_0 = 2$ for all the cases. The analytic results in the small bubble approximation, (22), (32), (36) appear in black continuous lines. The three insets compare the analytic small bubble results (black continuous line) with numerical simulations using $C_1 = 1$ and $C_2 = -0.5$ (purple +).

the p -th zero of $J_\alpha(x)$. The constant A is determined by requiring $\psi_p(x)$ to be normalized. On using the identity, $\int_0^a d\rho \rho J_\alpha(u_{\alpha p} \rho/a) J_\alpha(u_{\alpha q} \rho/a) = \delta_{p,q} (a^2/2) [J_{\alpha+1}(u_{\alpha p})]^2$ [31], we finally get

$$\psi_p(x) = \frac{\sqrt{2x}}{M|J_{\alpha+1}(u_{\alpha p})|} J_\alpha\left(\frac{u_{\alpha p}x}{M}\right), \quad (41)$$

and the probability

$$W_L \propto \left(\frac{x_0}{M-\epsilon}\right)^{C_1} \frac{2\sqrt{(M-\epsilon)x_0}}{M^2} \times \sum_{p=1}^{\infty} \frac{e^{-u_{\alpha p}^2 t_m/(2M^2)}}{[J_{\alpha+1}(u_{\alpha p})]^2} J_\alpha\left(\frac{u_{\alpha p}(M-\epsilon)}{M}\right) J_\alpha\left(\frac{u_{\alpha p}x_0}{M}\right). \quad (42)$$

Next, we evaluate W_L to leading order in ϵ by Taylor expanding $J_\alpha\left(\frac{u_{\alpha p}(M-\epsilon)}{M}\right)$ and also using the result $J'_\alpha(u_{\alpha p}) = -J_{\alpha+1}(u_{\alpha p})$, which follows from the following identity: $J'_\alpha(z) = \frac{\alpha}{z} J_\alpha(z) - J_{\alpha+1}(z)$ [30]. We finally get

$$W_L \propto \epsilon \frac{2x_0^{C_1+1/2}}{M^{C_1+5/2}} \sum_{p=1}^{\infty} u_{\alpha p} \frac{e^{-u_{\alpha p}^2 t_m/(2M^2)}}{J_{\alpha+1}(u_{\alpha p})} J_\alpha\left(\frac{u_{\alpha p}x_0}{M}\right) + \mathcal{O}(\epsilon^2). \quad (43)$$

The probability $P(M, t_m; \epsilon)$ of the whole path is the product of (43) and (38) with a normalization constant $B(\epsilon)$, which is determined by requiring that $\lim_{\epsilon \rightarrow 0} \int_0^\infty P(M, t_m; \epsilon) dt_m \rightarrow P(M)$, where $P(M)$ is given by Eq. (36),

$$P(M, t_m; \epsilon) = B(\epsilon) W_L W_R. \quad (44)$$

Using the identity $\sum_{p=1}^{\infty} J_\alpha(u_{\alpha p} x_0/M)/(u_{\alpha p} J_{\alpha+1}(u_{\alpha p})) = x_0^\alpha/(2M^\alpha)$ for $0 \leq x_0 < M$ [36], we get $B(\epsilon) = \frac{1}{2\epsilon^2} \left(\frac{x_0}{M}\right)^{C-C_1-1/2}$, where $C = 2C_1 + 1 - \sqrt{1+4C_1^2}/2$. Substituting for $B(\epsilon)$ in Eq. (44) and taking the limit $\epsilon \rightarrow 0$, we get the desired probability,

$$P(M, t_m) = (2C_1 + 1) \frac{x_0^C}{M^{C+3}} \times \sum_{p=1}^{\infty} u_{\alpha p} \frac{e^{-u_{\alpha p}^2 t_m/(2M^2)}}{J_{\alpha+1}(u_{\alpha p})} J_\alpha\left(\frac{u_{\alpha p}x_0}{M}\right). \quad (45)$$

For the free Brownian motion, taking $C_1 = 0$, this result reduces to that derived in [23].

IV. LARGE BUBBLE DYNAMICS

We study here the dynamics of large bubbles of size $x > x_{\text{ch}}$, see Eq. (5). In this limit, one can neglect the term $-C_1/x$ in the Langevin equation (3), and study the dynamics dictated by

$$\frac{dx}{dt} = C_2 + \tilde{\xi}(t). \quad (46)$$

This equation describes a one-dimensional random walk, $x(t)$, in the presence of a constant drift, C_2 . The probability distribution to find a bubble of size x at time t is a shifted Gaussian $P(x, t) \sim e^{-(x-x_0-C_2t)^2/2t}$, where x_0 is the initial size of the bubble. Below the melting temperature ($C_2 < 0$), the bubble shrinks and eventually disappears in time. Above T_m , when $C_2 > 0$, the bubble grows in size as time passes. For large $C_2 > 0$, the first-passage time diverges. Thus, our analysis below of various first-passage functionals is valid for large bubbles at temperatures below T_m as well as above T_m , in the latter case while conditioned on a finite t_f .

For obtaining the pdfs, $P(t_f|x_0)$ and $P(A|x_0)$, we adopt the BFP method. The relevant differential equation is obtained from Eq. (9) by substituting $C_1 = 0$,

$$\frac{1}{2} \frac{d^2 Q(x_0)}{dx_0^2} + C_2 \frac{dQ(x_0)}{dx_0} - pU(x_0)Q(x_0) = 0, \quad (47)$$

with the boundary conditions (i) $Q(x_0 \rightarrow \infty) = 0$, and (ii) $Q(x_0 \rightarrow 0) = 1$. We also derive analytical results for $P(M)$ and $P(M, t_m)$.

A. First-passage time distribution: $P(t_f|x_0)$

This distribution has already been investigated in [35] in a different context. We thus omit the details of the calculation, but include the results for the sake of completeness of our presentation. The procedure involves solving Eq. (47) with $U(x_0) = 1$ under the boundary conditions, then taking inverse Laplace transform of the solution to yield

$$P(t_f|x_0) = \frac{1}{\sqrt{2\pi}} \frac{x_0}{t_f^{3/2}} \exp \left[-\frac{(x_0 + C_2 t_f)^2}{2t_f} \right]. \quad (48)$$

The moments $\langle t_f^k \rangle$ may be obtained by using the identity, $\int_0^\infty x^{\nu-1} e^{-\beta/x - \gamma x} dx = 2(\beta/\gamma)^{\nu/2} K_\nu(2\sqrt{\beta\gamma})$ for $\text{Re}(\beta) > 0$ and $\text{Re}(\gamma) > 0$, where $K_\nu(x)$ is the modified Bessel function of the second kind [30]. One gets

$$\langle t_f^k \rangle = \sqrt{\frac{2}{\pi}} \left(\frac{x_0}{|C_2|} \right)^k (x_0 |C_2|)^{1/2} e^{-C_2 x_0} K_{k-1/2}(|C_2| x_0). \quad (49)$$

Noting that $K_{1/2}(x) = \sqrt{\pi/(2x)} e^{-x}$, the mean first-passage time is given by $\langle t_f \rangle = x_0 e^{-2C_2 x_0} / C_2$ for $C_2 > 0$, and by $\langle t_f \rangle = x_0 / |C_2|$ for $C_2 < 0$. The survival probability, defined in Eq. (24), is given by

$$C(x_0, t) = 1 - \frac{x_0}{\sqrt{2\pi}} e^{-C_2 x_0} \int_0^t t_f^{-3/2} e^{-x_0^2/(2t_f) - C_2^2 t_f/2} dt_f. \quad (50)$$

For $C_2 < 0$ ($T < T_m$) and for large t , one has $C(x_0, t) \approx 1 - (C_2 x_0) / (2\sqrt{\pi}) e^{-C_2 x_0 - x_0^2/(2t)} \left[\Gamma(-1/2) - \Gamma(-1/2, C_2^2 t/2) \right]$. Using the result that $\Gamma(s, x) \rightarrow$

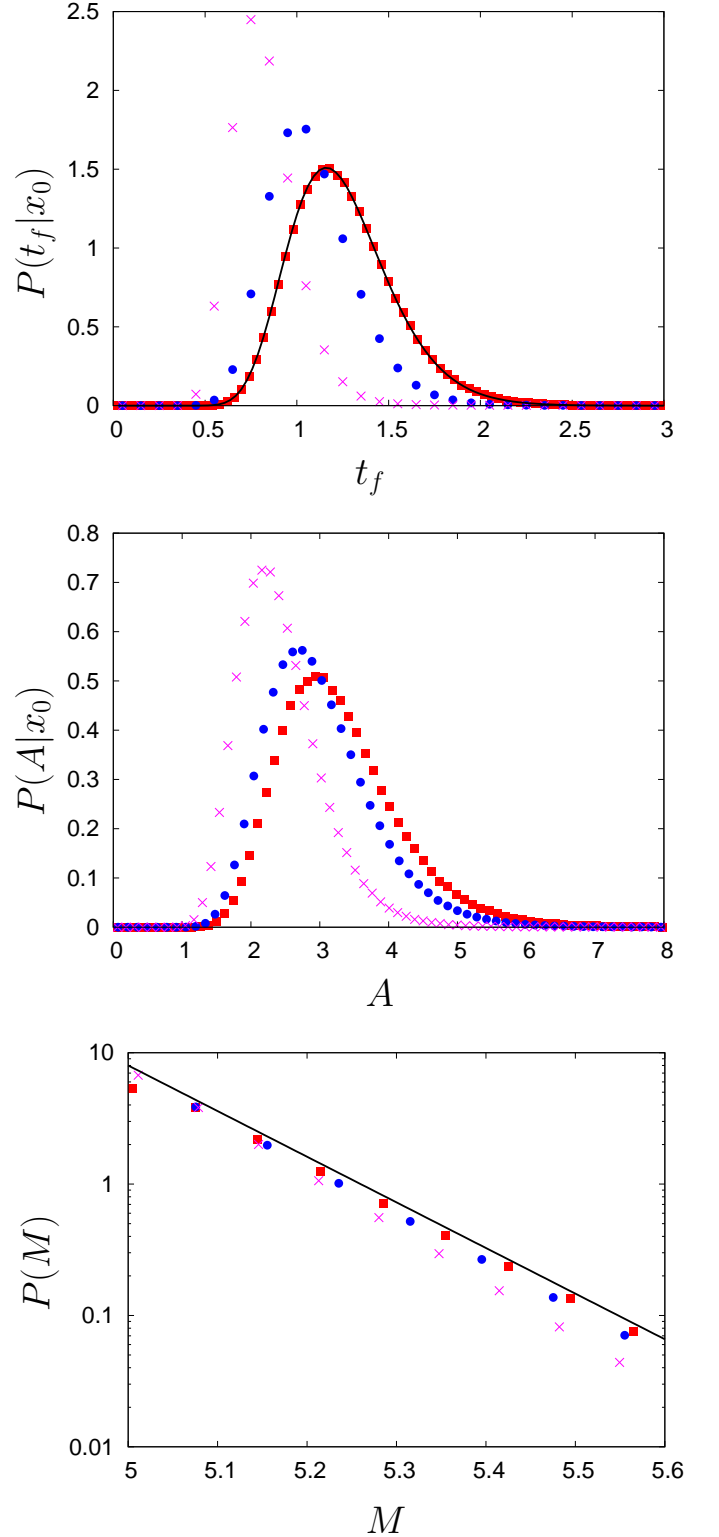


FIG. 4: (Color online) Results from numerical simulations below the melting temperature for the pdf of the first-passage time (top), the pdf of the area till the first-passage time (center), and the pdf of the maximum size till the first-passage time pdf (bottom). The parameters are $C_1 = 0$ (red square), $C_1 = 1$ (blue dots), and $C_1 = 4$ (purple cross). The initial bubble size is $x_0 = 5$ and $C_2 = -4$ in all the cases. The analytic results in the large bubble approximation appear in black continuous lines. In the middle panel, we do not make a comparison with the analytic function for $P(A|x_0)$ since its explicit form is known only in the limit of small and large values of A .

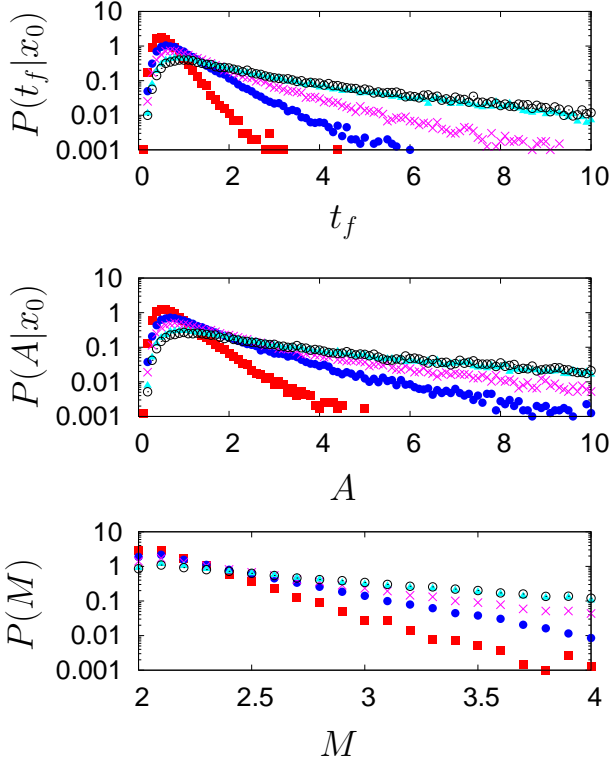


FIG. 5: (Color online) Results from numerical simulations below and above T_m , showing the first-passage time pdf (top), the pdf of the area till the first-passage time (center), and the pdf of the maximum till the first-passage time (bottom). The parameters are $C_2 = -2$ (red filled square), $C_2 = -1$ (blue filled circle), $C_2 = -0.5$ (purple cross), $C_2 = 0.1$ (light blue filled triangle), and $C_2 = 0.5$ (black circle). The initial bubble size is $x_0 = 2$ and $C_1 = 1$ in all cases.

$x^{s-1}e^{-x}$ as $x \rightarrow \infty$ [31], we get $C(x_0, t) \sim \sqrt{2/\pi}(x_0/C_2^2)t^{-3/2} \exp[-(x_0 - |C_2|t)^2/(2t)]$.

Figure 4 compares the analytic result for $P(t_f|x_0)$ with numerical simulations obtained by considering the full potential. Since, for $x_0 > x_{ch}$ with $C_2 > 0$, many trajectories have diverging t_f , we performed here numerical simulations only below the melting temperature, so that $C_2 < 0$. In this case, with increasing $|C_2|$, the effective drift velocity towards bubble closure increases and bubbles quickly disappear in time. The top panel demonstrates that the analytical prediction (48) agrees with simulation results for $x_0 > x_{ch}; C_2 < 0$. Figure 5 further includes results from numerical simulations by considering the full bubble potential, displaying the behaviors both below and above the melting temperature. Upon increasing C_2 from negative values (i.e., for $T < T_m$) to positive values (i.e., for $T > T_m$), one notes that (i) the center of the pdf $P(t_f|x_0)$ is displaced to longer times, and that (ii) the bubble lifetime is significantly enhanced (see Fig. 5, top panel). This corroborates with the physical picture that with increasing temperature, a bubble takes a longer time to disappear.

B. Distribution of the area till the first-passage time: $P(A|x_0)$

This quantity can be obtained by solving Eq. (47) with $U(x_0) = x_0$ with the appropriate boundary conditions, then deriving the inverse Laplace transform of the solution, see [35, 37] for details. In particular, one obtains the following two limiting behaviors of the distribution $P(A|x_0)$: For $A \rightarrow \infty$, one has

$$P(A|x_0) \approx \frac{e^{-C_2 x_0} \sinh(|C_2| x_0)}{\sqrt{\pi}} \left(\frac{2}{3}\right)^{1/4} \left(\frac{|C_2|}{A}\right)^{3/4} \times \exp\left\{-\left(\frac{8}{3}\right)^{1/2} |C_2|^{3/2} A^{1/2}\right\}. \quad (51)$$

In the opposite $A \rightarrow 0$ limit, one gets [37]

$$P(A|x_0) \approx \frac{2^{1/3}}{3^{2/3}\Gamma(1/3)} \frac{x_0 e^{-C_2 x_0}}{A^{4/3}} e^{-2x_0^3/9A}. \quad (52)$$

Note the distinct asymptotic forms in Eqs. (51) and (52). While the latter demonstrates a behavior similar to that observed in the small bubble dynamics [cf. Eq. (32)], the former predicts a different scaling behavior.

Results from numerical simulations are displayed in Figs. 4 - 5. For a fixed value of $C_2 < 0$, on increasing C_1 , Fig. 4 shows the narrowing of $P(A|x_0)$ and the displacement of its center towards smaller A values, thereby reflecting the increased importance of the entropy term in the free energy function. On fixing C_1 and on increasing C_2 from negative to (small) positive values, the area pdf develops an increasing contribution at large A values, thereby hinting at the onset of large bubbles and long first-passage times when $T > T_m$.

C. Distribution of the maximum before the first-passage time: $P(M)$

The procedure here proceeds as in Section III C. One first finds the cumulative probability $q(x_0)$, which satisfies [23, 35]

$$\frac{1}{2} \frac{d^2 q(x_0)}{dx_0^2} + C_2 \frac{dq(x_0)}{dx_0} = 0. \quad (53)$$

With the boundary conditions (i) $q(0) = 1$ and (ii) $q(M) = 0$, this gives the solution

$$q(x_0) = \frac{e^{-C_2 x_0} \sinh[C_2(M - x_0)]}{\sinh(C_2 M)}. \quad (54)$$

The desired pdf is obtained as the derivative of $q(x_0)$ with respect to M ,

$$P(M) = \frac{C_2 e^{-C_2 x_0} \sinh(C_2 x_0)}{\sinh^2(C_2 M)}; \quad M \geq x_0. \quad (55)$$

This result has been obtained in [23, 35] in a different context. Figure 4 compares this form with numerical results at temperatures below T_m ($C_2 < 0$). We observe a good agreement for initial bubble sizes satisfying $x_0 > x_{\text{ch}}$. Figure 5 further displays numerical results, both below T_m and above it, by adopting the full bubble potential.

D. Joint pdf of the maximum M and the corresponding time t_m before the first-passage time:
 $P(M, t_m)$

This distribution has been studied in [23] for the random motion (46) with $C_2 < 0$ by employing the PD method described in Section II D. To compute $P(M, t_m)$ for general C_2 , we follow the discussion of Section III D and split a representative path into two parts, before and after t_m . We compute the weight of each part separately. The weight W_R of the path after t_m is given by $W_R = q(M - \epsilon)$. Using Eq. (54), and then taking ϵ to be infinitesimally small, we get

$$W_R = \frac{e^{-C_2(M-\epsilon)} \sinh(C_2\epsilon)}{\sinh(C_2M)} = \epsilon \frac{C_2 e^{-C_2M}}{\sinh(C_2M)} + \mathcal{O}(\epsilon^2). \quad (56)$$

The weight W_L of the part before t_m is obtained from Eq. (15) by substituting $C_1 = 0$,

$$W_L \propto e^{C_2(M-\epsilon-x_0)} \sum_{p=1}^{\infty} e^{-E_p t_m} \psi_p(M-\epsilon) \psi_p(x_0). \quad (57)$$

Here, $\psi_p(x)$ and $E_p(x)$ are the eigenfunctions and energies of the Hamiltonian (13) with the potential,

$$V(x) = \begin{cases} \frac{C_2^2}{2} & \text{if } 0 < x < M, \\ \infty & \text{if } x = 0, x = M. \end{cases} \quad (58)$$

The normalized eigenfunctions are easily obtained as $\psi_p(x) = \sqrt{2/M} \sin(p\pi x/M)$ with the corresponding energies $E_p = C_2^2/2 + p^2\pi^2/(2M^2)$. Substituting this in Eq. (57), we get

$$W_L \propto \epsilon e^{C_2(M-x_0)-C_2^2 t_m/2} \frac{2\pi}{M^2} \times \sum_{p=1}^{\infty} (-1)^{p+1} p \sin\left(\frac{p\pi x_0}{M}\right) e^{-p^2\pi^2 t_m/(2M^2)} + \mathcal{O}(\epsilon^2). \quad (59)$$

The last equation, together with Eq. (56), gives the total probability,

$$P(M, t_m; \epsilon) = B(\epsilon) W_L W_R. \quad (60)$$

The normalization constant $B(\epsilon)$ is determined by requiring that $\lim_{\epsilon \rightarrow 0} \int_0^\infty P(M, t_m; \epsilon) dt_m \rightarrow P(M)$, given in Eq. (55). With $\sum_{p=1}^{\infty} (-1)^{p-1} p \sin(px)/(p^2 + a^2) = (\pi/2) \sinh(ax)/\sinh(a\pi)$ for $-\pi < a < \pi$ [30], one gets $B(\epsilon) = 1/2\epsilon^2$. Using this expression for $B(\epsilon)$ in Eq. (60) and taking the limit $\epsilon \rightarrow 0$, we get the desired pdf,

$$P(M, t_m) = \frac{C_2 e^{-C_2 x_0 - C_2^2 t_m/2}}{\sinh(C_2 M)} \frac{\pi}{M^2} \times \sum_{p=1}^{\infty} (-1)^{p+1} p \sin\left(\frac{p\pi x_0}{M}\right) e^{-p^2\pi^2 t_m/(2M^2)}. \quad (61)$$

The marginal distribution $P(t_m)$ can be obtained by integrating $P(M, t_m)$ over M from x_0 to infinity. The large- t_m and small- t_m asymptotic behaviors of $P(t_m)$ for $C_2 < 0$ are discussed in [23].

Quantities	Results for small bubble	Results for large bubble
$P(t_f x_0)$	$\sim t_f^{-C_1-3/2} e^{-x_0^2/2t_f}$ $\sim t_f^{-C_1-3/2} ; \quad t_f \rightarrow \infty$ $\sim e^{-x_0^2/2t_f} ; \quad t_f \rightarrow 0$	$\sim t_f^{-3/2} e^{-(x_0+C_2t_f)^2/2t_f}$ $\sim t_f^{-3/2} e^{-C_2x_0} e^{-C_2^2t_f/2} ; \quad t_f \rightarrow \infty$ $\sim e^{-(x_0+C_2t_f)^2/2t_f} ; \quad t_f \rightarrow 0$
$C(x_0, t)$	$\sim t^{-C_1-1/2} ; \quad t \rightarrow \infty$ $\approx 1 - \frac{(x_0^2/2)^{C_1-1/2}}{\Gamma(C_1+1/2)} t^{1/2-C_1} e^{-x_0^2/2t} ; \quad t \rightarrow 0$	$\sim t^{-3/2} e^{-\left[\frac{(x_0-C_2t)^2}{2t}\right]} ; \quad t \rightarrow \infty$
$P(A x_0)$	$\sim A^{-\frac{2}{3}(C_1+2)} e^{-2x_0^3/9A}$ $\sim A^{-\frac{2}{3}(C_1+2)} ; \quad A \rightarrow \infty$ $\sim e^{-2x_0^3/9A} ; \quad A \rightarrow 0$	$A^{-3/4} e^{-\left(\frac{8}{3}\right)^{1/2} C_2 ^{3/2} A^{1/2}} ; \quad A \rightarrow \infty$ $\sim A^{-4/3} e^{-2x_0^3/9A} ; \quad A \rightarrow 0$
$P(M)$	$\sim M^{-2C_1-2}$	$\sim \frac{1}{\sinh^2(C_2M)}$
$P(M, t_m)$	$\sim M^{-(C+3)} \sum_{p=1}^{\infty} u_{\alpha p} \frac{e^{-u_{\alpha,p}^2 t_m/2M^2}}{J_{\alpha+1}(u_{\alpha p})} J_{\alpha}\left(\frac{u_{\alpha,p} x_0}{M}\right),$ where $C = 2C_1 + 1 - \sqrt{1 + 4C_1^2}/2$	$\sim \frac{e^{-C_2^2 t_m/2}}{M^2 \sinh(C_2M)} \sum_{p=1}^{\infty} (-1)^{p+1} p \sin\left(\frac{p\pi x_0}{M}\right) e^{-p^2 \pi^2 t_m/2M^2}$

Table 1: Scaling behavior of the probability distribution functions of various Brownian functionals calculated in this work for small and large DNA bubbles.

V. CONCLUSIONS

In this paper, we derived probability distribution functions of various Brownian functionals associated with a random walk model for DNA bubble dynamics at temperatures below, at, and above the denaturation temperature. Based on the backward Fokker-Planck method discussed in [22], we derived (i) the first-passage time distribution $P(t_f|x_0)$, providing information about the bubble lifetime, (ii) the distribution $P(A|x_0)$, of the area A covered by the random walk till the first-passage time, measuring the bubble reactivity to processes within the DNA, and (iii) the distribution $P(M)$, of the maximum bubble size M before bubble closure, all conditioned on an initial bubble of size x_0 ($x_0 \in [0, M]$). (iv) The joint probability distribution $P(M, t_m)$ of the maximum bubble size M and the time t_m of its occurrence before the first passage time was also obtained by employing the Feynman-Kac path integral formulation. The advantage of the elegant methods adopted here is that they produce results on various functionals by making proper choices of a single term in a parent differential equation with

appropriate boundary conditions.

We considered separately the dynamics of small and large bubbles. Analytical results for the pdfs at each limit nicely agree with Langevin simulations. Our analysis reveals different nontrivial scaling behaviors of $P(t_f|x_0)$, $P(A|x_0)$, $P(M)$ and $P(M, t_m)$, as summarized in Table 1. The scaling exponents are characterized either by the entropic parameter C_1 , or by the base-pair dissociation parameter C_2 . These quantities may thus be estimated experimentally by using fluorescence correlation spectroscopy [8] to measure, e.g., the maximum size distribution $P(M)$ for small and large bubbles separately.

We expect our results to be useful in quantifying chemical processes within DNA, for example, protein binding to single-stranded DNA, and for developing a deeper understanding of polymer dynamics. It is of interest to extend our study and consider loop-loop interactions [27], and the effects of disorder and heterogeneity in predicting the kinetics of specific processes within DNA bubbles [38–41].

Acknowledgments

DS and MB acknowledge support from the Connaught fund and from NSERC. SG thanks Amir Bar, Raphaël Chetrite, Ori Hirschberg, Satya N. Majumdar and David

Mukamel for fruitful discussions and suggestions, and gratefully acknowledges the Israel Science Foundation (ISF) for supporting his research at the Weizmann Institute of Science.

-
- [1] J. D. Watson and F. H. C. Crick, Cold Spring Harb. Symp. Quant. Biol. **18**, 123 (1953).
 - [2] A. Kornberg and T. A. Baker, *DNA Replication Second Edition* (University Science Books, Sausalito, California, 2005).
 - [3] M. D. Frank-Kamenetskii, Phys. Rep. **288**, 13 (1997).
 - [4] R. M. Wartell and A. S. Benight, Phys. Rep. **126**, 67 (1985).
 - [5] D. Poland and H. A. Scheraga, *Theory of Helix-Coil Transitions in Bio-Polymers* (Academic Press, New York, 1970).
 - [6] C. Danilowicz, Y. Kafri, R. S. Conroy, V. W. Coljee, J. Weeks, and M. Prentiss, Phys. Rev. Lett. **93**, 078101 (2004).
 - [7] O. Krichevsky and G. Bonnet, Rep. Prog. Phys. **65**, 251 (2002).
 - [8] G. Altan-Bonnet, A. Libchaber, and O. Krichevsky, Phys. Rev. Lett. **90**, 138101 (2003).
 - [9] J. Phys.: Condens. Matter, Special Section on DNA melting **21** (2009).
 - [10] R. Metzler, T. Ambjörnsson, A. Hanke, and H. C. Fogedby, J. Phys.: Condens. Matter **21**, 034111 (2009), and references therein.
 - [11] H. Kunz, R. Livi, and A. Sütö, J. Stat. Mech.: Theory Exp. P06004 (2007).
 - [12] T. Ambjörnsson, S. K. Banik, M. A. Lomholt, and R. Metzler, Phys. Rev. E **75**, 021908 (2007).
 - [13] S. K. Banik, T. Ambjörnsson, and R. Metzler, Europhys. Lett. **71**, 852 (2005).
 - [14] A. Hanke, and R. Metzler, J. Phys. A: Math. Gen. **36**, L473 (2003).
 - [15] A. Bar, Y. Kafri, and D. Mukamel, Phys. Rev. Lett. **98**, 038103 (2007).
 - [16] A. Bar, Y. Kafri, and D. Mukamel, J. Phys.: Condens. Matter **21**, 034110 (2009).
 - [17] T. Dauxois, M. Peyrard, and A. R. Bishop, Phys. Rev. E **47**, 684 (1993).
 - [18] S. Srivastava and Y. Singh, Europhys. Lett. **85**, 38001 (2009).
 - [19] H. C. Fogedby and R. Metzler, Phys. Rev. Lett. **98**, 070601 (2007); Phys. Rev. E **76**, 061915 (2007).
 - [20] L.-A. Wu, S. S. Wu, and D. Segal, Phys. Rev. E **79**, 061901 (2009).
 - [21] Note that we refer to the functionals here as “Brownian functionals”, although the dynamics involves both the random delta-correlated force and a deterministic component corresponding to the bubble potential, see Eq. (1).
 - [22] S. N. Majumdar, Current Science **89**, 2076 (2005).
 - [23] J. Randon-Furling and S. N. Majumdar, J. Stat. Mech.: Theory Exp. P10008 (2007).
 - [24] M. Kac, Trans. Am. Math. Soc. **65**, 1 (1949).
 - [25] S. N. Majumdar and M. J. Kearney, Phys. Rev. E **76**, 031130 (2007).
 - [26] P. L. Krapivsky, S. N. Majumdar and A. Rosso, J. Phys. A: Math. Theor. **43**, 315001 (2010).
 - [27] Y. Kafri, D. Mukamel, and L. Politi, Physica A **306**, 39 (2002).
 - [28] As discussed in [23], one is required to impose an infinitesimal cut-off ϵ , or else an infinite number of crossings of the level M (immediately after the first contact at time t_m) would make it impossible to ensure that the path stays below M at times subsequent to t_m .
 - [29] A. C. Brańka and D. M. Heyes, Phys. Rev. E **58**, 2611 (1998).
 - [30] I. S. Gradshteyn and I. M. Ryzhik, *Tables of Integrals, Series, and Products* (Academic Press, New York, 1965).
 - [31] G. B. Arfken and H. J. Weber, *Mathematical Methods for Physicists Fourth Edition* (Academic Press, London, 1995).
 - [32] *Tables of Integral Transforms, Volume I, Based, in part, on notes left by Harry Bateman and compiled by the staff of the Bateman Manuscript Project*, edited by A. Erdélyi, M. F. Oberhettinger and F. G. Tricomi (McGraw-Hill, New York, 1954).
 - [33] A. J. Bray, Phys. Rev. E **62**, 103 (2000).
 - [34] *Introduction to Bessel Functions*, F. Bowman (Dover, New York, 1958).
 - [35] M. J. Kearney and S. N. Majumdar, J. Phys. A: Math. Gen. **38**, 4097 (2005).
 - [36] A. P. Prudnikov, Yu. A. Brychkov and O. I. Marichev *Integrals and Series: Volume 2 Special Functions* (Gordon and Breach Science Publishers, Netherlands, 1998).
 - [37] M. J. Kearney, S. N. Majumdar, and R. J. Martin, J. Phys. A: Math. Theor. **40**, F863 (2007).
 - [38] B. Coluzzi and E. Yeramian, Eur. Phys. J. B **56**, 349 (2007).
 - [39] T. Ambjörnsson, S. K. Banik, O. Krichevsky, and R. Metzler, Phys. Rev. Lett. **97**, 128105 (2006).
 - [40] T. Ambjörnsson, S. K. Banik, O. Krichevsky, and R. Metzler, Biophys. J. **92**, 2674 (2007).
 - [41] M. Zoli, Phys. Rev. E **81**, 051910 (2010).